

EXPERIMENTAL INVESTIGATIONS ON THE COOLABILITY OF DEBRIS BEDS UNDER VARIATION OF INFLOW CONDITIONS

S. Leininger, R. Kulenovic and E. Laurien

University of Stuttgart

Institute of Nuclear Technology and Energy Systems (IKE)

Pfaffenwaldring 31, 70569 Stuttgart, Germany

Email of corresponding author: simon.leininger@ike.uni-stuttgart.de

ABSTRACT

In case of a severe accident, continuous unavailability of cooling water to the reactor core may result in over heating of the fuel elements and the loss of core integrity. Under such conditions, the molten core can relocate to the lower plenum of the reactor pressure vessel (RPV) and form a structure of heated particles of different sizes and shapes (debris) due to the possible presence of residual water. To avoid a remelting and in the further course of the accident a damage to the RPV it is of great importance to establish long-term coolability. If long-term coolability cannot be established a failure of the RPV and uncontrolled melt release would be the consequence. In this case for certain reactor types again a debris bed can be formed in the reactor cavity.

The DEBRIS test facility at IKE was established to investigate the coolability limits of such debris beds. The cylindrical bed (150 mm diameter, 640 mm height) is heated by an inductive heating system, which acts as a volumetric heat source. To investigate the thermohydraulic debris bed behavior the test section is equipped with 55 thermocouples and 8 differential pressure transducers. The maximum removable heat flux (dryout heat flux, DHF) from a debris bed can be determined by increasing the heat input in small increments.

This paper presents mainly the results of systematic boiling and dryout experiments at IKE. In contrast to IKE experiments in the past the focus is on debris beds consisting of non-spherical particles with well-defined geometries such as cylinders and screws to investigate the influence of the particle shape on the bed's coolability. For the current set of experiments, the cooling behavior of two kinds of particles was investigated under variation of system pressure (0.1, 0.3 and 0.5 MPa) and inflow condition. The debris bed was flooded either from top or simultaneously from top and from bottom by a natural circulation loop. Additionally, several downcomer configurations were investigated. The experimental results show that a downcomer can significantly improve the bed's coolability since the penetration of water into the bed is not limited by the counter-current flow limitation (CCFL).

KEYWORDS

reactor safety, severe accidents, debris beds, porous media, two-phase flow

1. INTRODUCTION

During a severe accident in a light water reactor the fuel elements can overheat due to insufficient heat removal of emerging decay heat. If water supply can be reestablished, the fuel elements can crack due to thermal shock or if the fuel elements cannot be cooled down, they can even melt and relocate to the lower core region or to the lower plenum, where the molten core material fragments either at still intact core

material or in residual water (in-vessel scenario). If long-term coolability cannot be established in this stage, the debris can remelt and threaten the integrity of the RPV. If the RPV is failing, uncontrolled melt release into the reactor cavity would be the consequence. For some reactor types (e. g. in Sweden and Finland) a flooding of the reactor cavity with water is foreseen for such scenario to break up the melt jet. Hence, again a particle debris bed can be formed (ex-vessel scenario), where long-term coolability can easier be achieved than for a high density agglomeration. Therefore, addressing the issue of coolability the behavior of heat generating debris beds is of prime importance in the framework of severe accident management strategies, particularly in the case of above mentioned late phase accident scenarios.

In order to remove the decay heat the bed may be flooded with coolant water either from top (top-flooding) or from bottom (bottom-flooding). Hence, a two-phase co- or counter-current flow establishes inside the bed. Due to the large surface area of porous media, the coolability of debris beds is normally not limited by the heat transfer from the particle to the coolant but by the availability of coolant inside the bed. In case of top-flooding, the uprising vapor can block the penetrating water from an overlaying water pool so that there is no sufficient water entering the bed to replace the evaporated water, which results in a dryout and as a consequence in an overheating of the bed. If the core is only partly damaged and the main structures in the RPV are still intact, injected water can be guided by the downcomer to the bottom of the degraded core. For an in-vessel scenario with relocated core material in the lower head of the RPV or an ex-vessel scenario, water will mainly penetrate into the bed from top but can also laterally enter the bed since a heap-like bed is considered for these scenarios.

In this context, boiling and dryout experiments are carried out to validate friction models in numerical simulations and to determine for instance the maximum removable heat flux (dryout heat flux, DHF) from a debris bed. E. g. Hofmann [1] has performed dryout experiments for top- and bottom-flooding conditions. For bottom-flooding, water was guided by an annulus gap from the top to the bottom of the bed. He pointed out the major differences between top- and bottom-flooding, which need to be considered in modelling. For top-flooding, no effect of the bed depth greater than 250 mm on the DHF was found for 3 mm particulate.

In previous studies at IKE, experiments were carried out under top- and bottom-flooding conditions by Schäfer et al. [2] and Rashid et al. [3] using the DEBRIS test facility. The focus was on the determination of pressure gradients and DHF with variation of inflow velocity of the coolant fluid (water), system pressure and bed composition (mono- and polydispersed beds with spherical particles, PREMIX particles [4]). They have found a strong increase of DHF with increasing system pressure and water injection rate from bottom. Rashid et al. already employed a downcomer (10 mm ID) for boiling and dryout experiments for system pressures up to 0.5 MPa. They found that a downcomer can increase the DHF by a factor of 2. A perforation of the downcomer was expected to improve further the coolability, because water can also penetrate laterally into the bed. The DHF was surprisingly not significantly higher than for pure top-flooding. This may be due to vapor, which penetrates into the downcomer and therefore is decreasing the flow cross-section of down-flowing water.

Atkhen et al. [5] performed dryout experiments in the SILFIDE facility. Steel beads were heated inductively and flooded both from top and from bottom. The experiments have also shown that bottom injection is at least two times more efficient than top coolant injection.

Li et al. [6] performed experiments in the POMECO-HT facility with focus on the DHF and the position of its first occurrence. They found that bottom injection improves the coolability and the dryout position is moving upwards with higher injection rate.

Konovalikhin et al. [7] carried out dryout experiments in both homogeneous and stratified beds with and without downcomer installation. They varied the number and total cross-section of downcomers to study

the effect of inflow condition on the DHF. They determined an increase of DHF by 50 - 600 % depending on the composition of the bed and on the flow cross-section of the downcomer.

Nayak et al. [8] performed reflooding experiments of a radially stratified bed employing downcomers. They installed a large downcomer (54 mm ID) in the bed centre and six smaller downcomers (9.5 mm ID) in the periphery. In their experiments different combinations of these downcomers were tested in order to study the effect of their location and size on quenching. It was found, that the accumulated flow area of the downcomers has a significant effect on the total quenching time.

Yang and Sehgal [9] have determined DHFs of axially stratified debris beds with and without an internal downcomer. They found that the enhancement of the DHF by the application of a central downcomer is higher for a small layer of low permeability particles on top. With increasing thickness ratio the improvement of a downcomer is reducing from about 155 % to less than 70 %. Furthermore, they showed that the enhancement of the DHF by a downcomer is increasing with increasing porosity of the top layer.

The focus of this paper is on the effect of inflow condition on the steady-state boiling and dryout behavior of heat generating debris beds. The bed is flooded in the DEBRIS test facility both from top and from bottom but also laterally by the installation of different downcomers. The bed consists of non-spherical particles with well-defined geometries in order to investigate the effect of the particles shape (see also [10]). Applying these particles a large bandwidth of porosity (0.38 - 0.58) can be covered. Spencer et al. [11] and Karbojian et al. [12] approved in corium fragmentation experiments that porosities in this range or even higher can occur. The conducted experiments can be used for validation of IKE's simulation code MEWA-3D, which is implemented in the German system code ATHLET-CD.

2. DEBRIS TEST FACILITY

The DEBRIS test facility at IKE (Figure 1) consists of a pressure vessel designed for pressures up to 4 MPa in which the cylindrical test section filled with particles is mounted. The pressure vessel is connected to a storage tank filled with preconditioned water and a pumping system, which allows performing boiling experiments with feeding water to the crucible at the bottom (bottom-flooding) or at the top (top-flooding). Furthermore, water can be fed to the bottom of the bed by an external natural circulation loop (external downcomer), which interconnects the water pool above the bed and the bottom of the bed (Figure 2). Additionally, multidimensional inflow conditions can be investigated by the installation of a downcomer (see section 3). For top- and bottom-flooding as well as for the external downcomer, the flow rate can be measured by two magnetic-inductive flow meters. The debris bed is volumetrically heated by an oil-cooled 2-winding induction coil connected to an RF-generator. The RF-generator operates at a maximum frequency of 300 kHz and has a nominal output power of 140 kW. The generated vapor is condensed by a condenser and restored in the storage tank. To replace the evaporated water for the downcomer configurations water is fed continuously from the top. The formed water pool above the bed is maintained at a constant level by an overflow (water return line).

The test section consists of a crucible made from material PTFE (Teflon) (Figure 2). It has a total height of about 810 mm and an inner diameter of 150 mm. The test section is equipped with 55 sheathed thermocouples (diameter 1 mm, type N), of which 51 are located in the debris bed on 25 levels at different radii and angular positions of the bed's cross-section. The thermocouples measure the temperature in the voids between the particles, which are filled with liquid, vapor or a mixture of both. Additionally, the test section is equipped with eight differential pressure transducers (10 kPa, class 0.1), which are connected to pressure taps at eight axial levels PL0 - PL7.

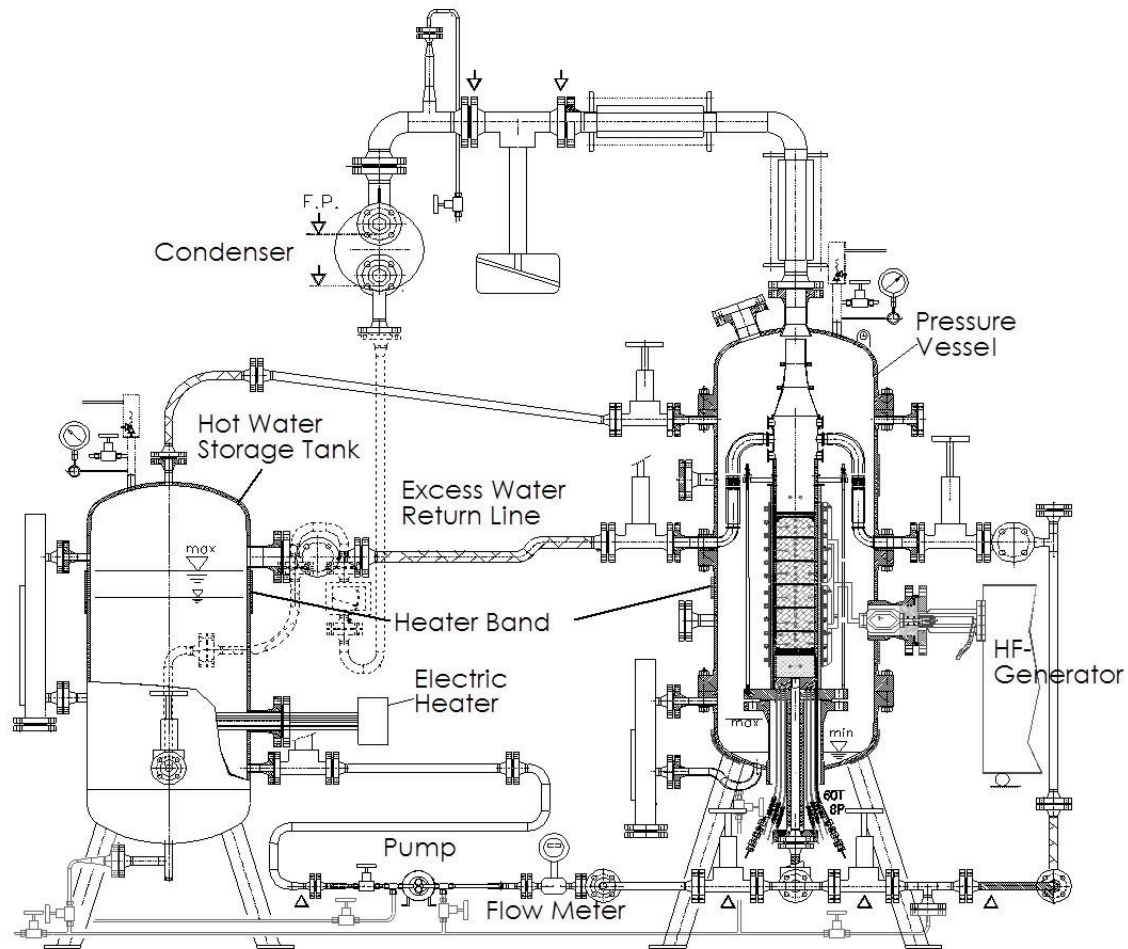


Figure 1. DEBRIS test facility

Two different kinds of particles, cylinders (length 5.75 mm, diameter 3 mm) and cylindrical screws (M3x10, ISO 1207), are used for the current set of experiments. The cylindrical particles are made of stainless steel and the screws of standard steel, which couples significantly better to the electromagnetic field induced by the inductive heating system. The effective diameters of the particles d_p were previously determined by fitting the Ergun equation [13] to pressure drop measurements in single-phase (liquid) experiments in a range of $Re_p \approx 0 - 70$ ($Re_p = \rho J d_p / \mu (1 - \varepsilon)$): Reynolds number in porous media with density ρ , superficial velocity J and dynamic viscosity μ of the liquid, bed porosity ε). They are $d_p = 3.0$ mm for cylinders and 2.8 mm for screws. The porosity of both beds is determined to $\varepsilon = 0.38$ and $\varepsilon = 0.58$, respectively. The bed height is 640 mm for all bed configurations with an additional water pool of 310 mm above the bed. At constant system pressure the bed is heated up to steady-state boiling condition at saturation temperature. Then, the heating power is increased in small steps until dryout is reached. A permanent increase of the bed temperature of 5 K above saturation temperature is defined as dryout. To avoid any damage to the PTFE crucible the maximum temperature is limited to 200 °C. Each power step is maintained for up to 20 minutes and each experiment is performed three times.

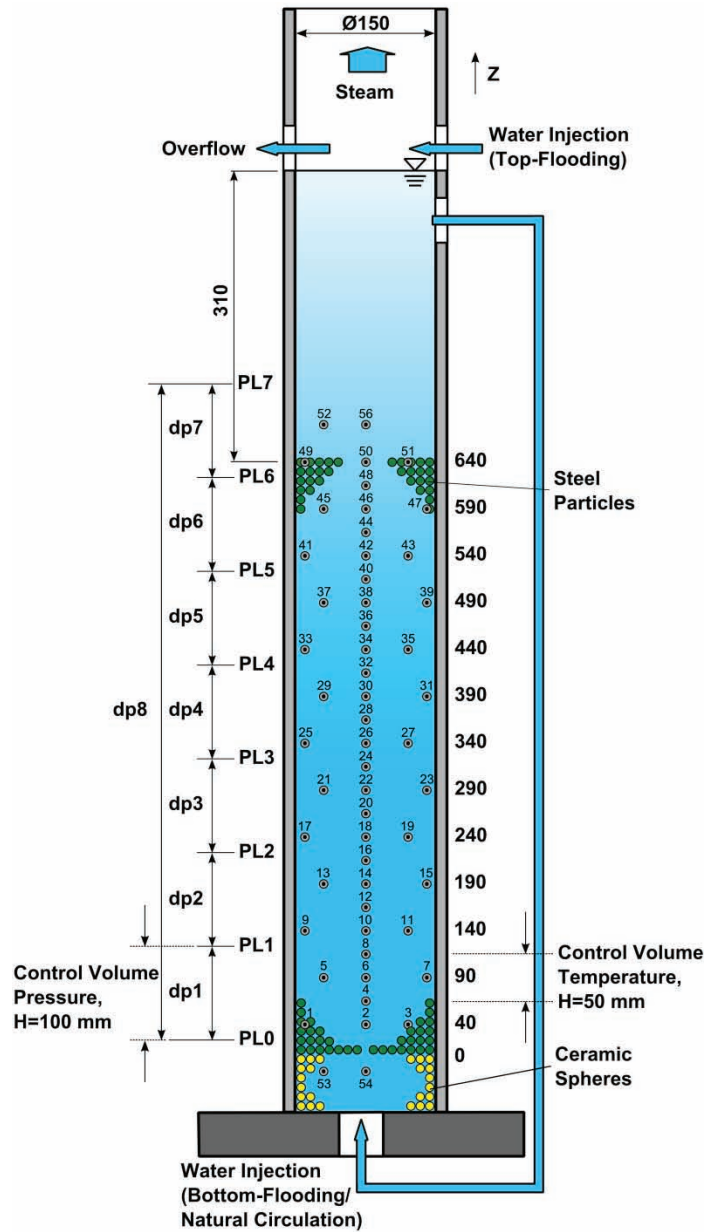
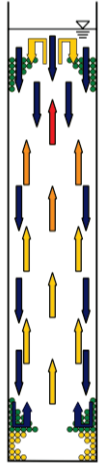
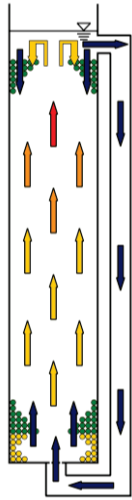
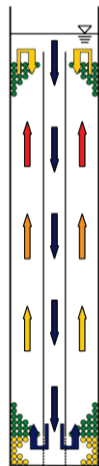
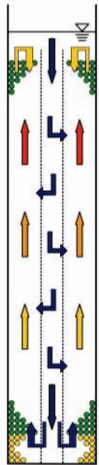
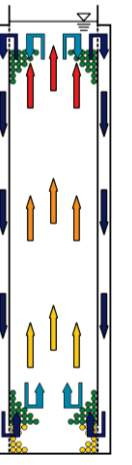
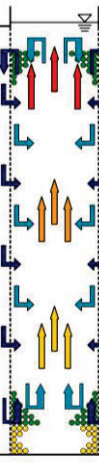


Figure 2. Position of thermocouples and pressure taps

3. VARIATION OF INFLOW CONDITION

For the current set of experiments, the boiling and dryout behavior of two homogeneous beds with strongly different permeability was investigated under variation of inflow condition (Table I). For top-flooding water is fed into the bed by an overlying water pool. The coolability of the bed is limited by the counter-current flow limitation (CCFL) since water has to penetrate into the bed from top and is in counter-current flow with uprising steam. By the installation of a downcomer, which is a pipe or channel with no particles in it ($\epsilon = 1$), a low resistance flow path is provided for feeding water. The idea of the downcomer is a separation of the phases water and steam, whereby water should flow downwards in the downcomer and steam should rise upwards in the bed.

Table I. Inflow configurations

<p>1) Top-flooding</p>  <ul style="list-style-type: none"> • No downcomer 	<p>2) External downcomer</p>  <ul style="list-style-type: none"> • Downcomer inner diameter: 25 mm • Minimum flow cross-section in downcomer: $\sim 322 \text{ mm}^2$ (at the bed's bottom) 	<p>3) Internal downcomer</p>  <ul style="list-style-type: none"> • Downcomer inner diameter: 10 mm • Flow cross-section in downcomer: $\sim 75 \text{ mm}^2$
<p>4) Perforated internal downcomer</p>  <ul style="list-style-type: none"> • Downcomer inner diameter: 10 mm • Flow cross-section in downcomer: $\sim 75 \text{ mm}^2$ • Perforated area: $\sim 11,200 \text{ mm}^2$ 	<p>5) Annular downcomer</p>  <ul style="list-style-type: none"> • Downcomer inner diameter: 180 mm • Downcomer outer diameter: 194 mm • Minimum flow cross-section in downcomer: $\sim 75 \text{ mm}^2$ (at inlet) 	<p>6) Perforated annular downcomer</p>  <ul style="list-style-type: none"> • Downcomer inner diameter: 180 mm • Downcomer outer diameter: 194 mm • Minimum flow cross-section in downcomer: $\sim 75 \text{ mm}^2$ (at inlet and every 100 mm in the downcomer) • Perforated area: $\sim 11,200 \text{ mm}^2$

In configuration 1, pure top-flooding by a 310 mm water pool is considered. The external downcomer (configuration 2) interconnects the water pool above the bed and the bottom of the bed, so water can be fed to the bottom of the bed by a natural circulation loop. In this configuration, the downcomer has the largest cross-section of all configurations but is reduced at the bottom of the bed by a net to prevent the particles from falling into the downcomer. The internal downcomer (configuration 3) is installed in the center of the bed and has a lower inner diameter compared to the external downcomer. The outlet of the downcomer is in the ceramic particle layer, so no steam can enter the downcomer. The perforated inner downcomer (configuration 4) has the same dimensions as the non-perforated version but is perforated along the complete height. To prevent the particles from falling into the downcomer the outer surface of the downcomer is covered by a net. The annular downcomer (configuration 5) is build up by a glass tube, which surrounds the test crucible. The so formed gap between test crucible and glass tube serves as a downcomer. Water can enter the downcomer at the bed's top and leaves it at the bed's bottom by holes in the test crucible. For the perforated annular downcomer (configuration 6), the test section is perforated along the bed height and covered by a net. Here, the perforated area is the same as for the perforated inner downcomer. Normally, the DHF for the annular downcomer configurations would be very high and exceed the capability of the heat generator. Since the cross-section cannot be reduced along the complete height due to constructive restrictions it is at least reduced at the inlet to obtain the same total cross-section as for the internal downcomer. For the perforated annular downcomer, the gap is additionally narrowed every 100 mm.

4. EXPERIMENTAL RESULTS

4.1. Determination of Heat Input

The heat input into the bed is calculated from the time-dependent increase in bed temperature dT/dt (sensible heating-up of coolant water) for different applied induction powers in a temperature range of 30 - 40 °C. The average temperature rise is used to estimate the power density of heat generation in the bed and coolant based on an adiabatic assumption:

$$dQ = [\varepsilon \cdot \rho_w \cdot c_p^w + (1 - \varepsilon) \cdot \rho_s \cdot c_p^s] \frac{dT}{dt} \quad (1)$$

where ε is the measured porosity of the particle bed, (ρ_w , ρ_s , c_p^w , c_p^s) are the densities and specific heat capacities of water and steel particles, respectively. Downward and lateral heat dissipation through an insulation layer of ceramic spheres (Figure 2) and the PTFE crucible is considered to be negligible. The effective heat flux q is defined as the integral heat generation:

$$q = Q \cdot h \quad (2)$$

where h is the total height of the bed. Figure 3 shows the calculated heat input data as well as the fitted curve for different power levels (heating level – RF-generator setting). It can be seen that the heat input is higher for screws compared to cylinders, which is due to different particle materials. The cylinders are made of stainless steel, whereas the screws are made of standard steel, which couples significantly better to the electromagnetic field. However, depending on the composition of the bed the maximum heat input is limited by the maximum voltage and/or current of the generator. For all inflow conditions, the same heat input curves are used. The effect of an internal downcomer on the heat input is considered as negligible since the downcomer covers less than 1.5 % of the bed's cross-section. The heat input curves are used to calculate the gas superficial velocity J_g (with bed cross-section A , liquid mass flow rate \dot{m} , heat of evaporation Δh_v , and saturation temperature T_s resp. subcooled temperature T_{in} of liquid):

$$J_g = \frac{q \cdot A - \dot{m} \cdot c_p^w \cdot (T_s - T_{in})}{A \cdot \Delta h_v \cdot \rho_g} \quad (3)$$

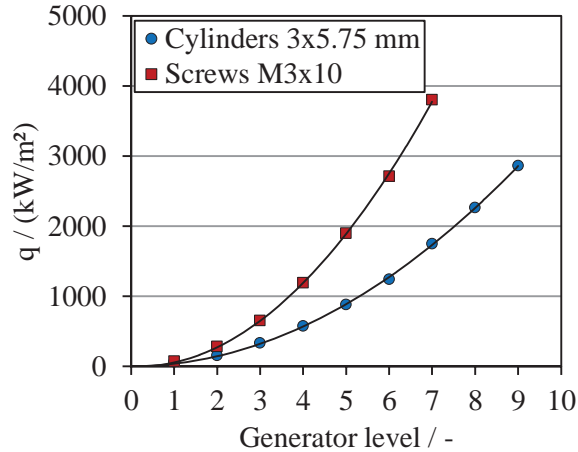


Figure 3. Heat input curves

4.2. Experimental Results at Boiling Condition below DHF

Boiling experiments for both cylindrical particles and screws were carried out under variation of system pressure (0.1, 0.3 and 0.5 MPa) and inflow condition (see Table I).

Figure 4 shows exemplary results of measured pressure gradients depending on the gas superficial velocity J_g for both beds and all inflow conditions at $p = 0.3$ MPa. Due to the interfacial friction the pressure gradient decreases at the beginning below the gradient of the hydrostatic water column. With increasing gas velocity the interfacial friction is declining and the total pressure gradient is rising. In the further course the fluid particle friction becomes more dominant and contributes mainly to the total pressure gradient. For high J_g , almost all water is evaporated. Thus, the complete cross-section can be occupied by steam. As a result, the fluid particle friction is decreasing. The measurement points in the diagrams are from three experiments with same boundary conditions. The error bars in vertical direction are due to uncertainties of the pressure transducers (100 Pa/m). For the horizontal error bars mainly uncertainties of the heat input determination and deviations in the system pressure, which is manually controlled, are considered. Small changes in system pressure have an effect on the fluid properties of water and steam, in particular on the steam density.

For top-flooding, water has to penetrate into the bed from top and is in counter-current flow with uprising steam. Therefore, the interfacial friction is dominant. With increasing J_g only a slight increase of the pressure gradient can be seen. Due to the low porosity of the cylindrical particles the fluid particle friction has a larger effect on the total pressure gradient inside the bed than for screws.

For the external downcomer configuration water can enter the bed both from top and from bottom driven by the lateral water column in the downcomer. Due to the improved access of water to the bed much higher steam velocities can be reached. The pressure gradient curves show that the pressure drop for low J_g is lower compared to pure top-flooding, which can be explained by lower interfacial friction since water and steam are mainly in co-current flow. For co-current flow, $J_g - J_l$ is lower than for counter-current flow.

In case of the internal downcomer, a higher pressure drop can be seen compared to the external downcomer. It can be assumed that the water superficial velocity is lower for the internal downcomer and thus the interfacial friction is higher. Furthermore, for low $J_g < 0.2$ m/s the curve is quite similar to the curve for top-flooding.

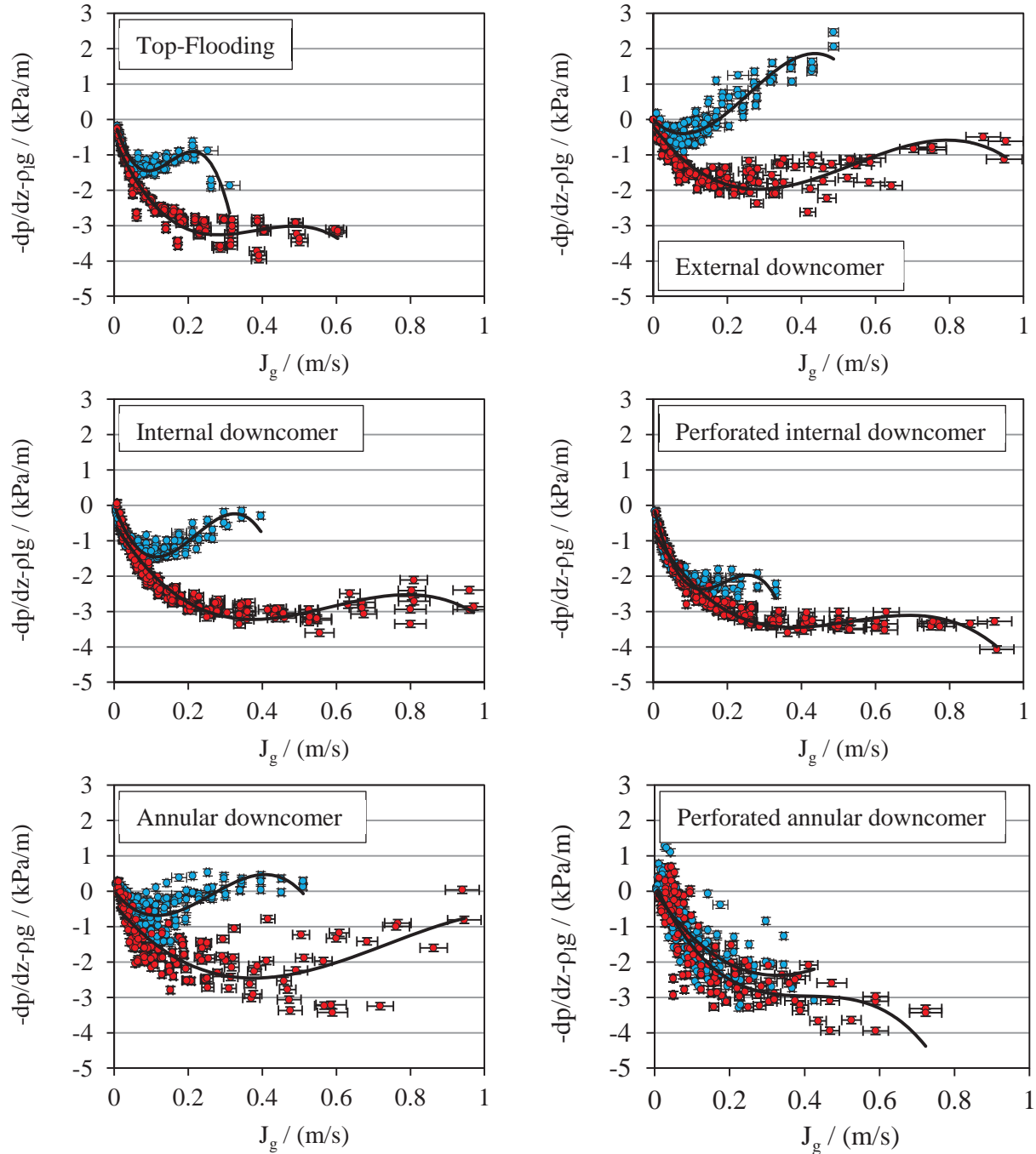


Figure 4. Measured pressure gradient for cylinders (blue) and screws (red) with variation of inflow condition at $p = 0.3$ MPa (solid line is a third order polynomial fit)

For the bed made of screws with perforated internal downcomer, the pressure gradients look almost identical to the non-perforated internal downcomer. Therefore, it can be assumed, that water penetrates into the bed in a similar way, i. e., via the downcomer and downwards inside the bed. For cylinders, the interfacial friction is higher than for the internal downcomer and it is even higher than for pure top-flooding, which is assumed to be the inflow condition with the highest interfacial friction. A possible

explanation is that due to the lateral flow condition no separated flow paths of water and steam can establish inside the bed, which increases the interfacial friction.

The pressure measurement for the annular downcomer shows an increased scattering, which is most likely due to evaporation of water inside the pressure measurement pipes since they are located inside the downcomer. Nevertheless, the curves show the typical S-shape and the values are in the same range as for the internal and external downcomer.

The same applies for the perforated annular downcomer. Here, the scattering was even stronger for some experiments, in particular at $p = 0.1$ MPa. For cylindrical particles, the curve is similar to the perforated internal downcomer. For screws, at least for low J_g the curve is similar to both internal downcomers.

In Figure 5 the measured total pressure difference along the bed height dp_8 (see Figure 2) as well as the inflow rate \dot{m} for the external downcomer configuration is depicted vs. the heat input q for cylindrical particles and screws for all applied system pressures. Generally, the pressure difference is decreasing at the beginning with increasing heat input q . For high q , the pressure difference is increasing since the fluid particle friction becomes dominant. Due to higher steam density the minimum of dp_8 is moving to higher q with increasing system pressure. Since dp_8 covers the pressure gradient in the water pool only in part and pressure losses in the downcomer are unknown the flow rate can't be calculated from the pressure difference dp_8 . Thus, pressure difference and flow rate can be compared only qualitatively.

For cylindrical particles, dp_8 is already increasing for quite low heat inputs since the fluid particle friction plays a significant role for porous beds with low porosity. Therefore, the inflow rate and in consequence the coolability of the particle bed is significantly lower compared to screws. In case of screws, the pressure gradient is only increasing for $p = 0.1$ MPa. For higher pressure, the gradient is remaining at a low level or even decreasing since the fluid particle friction is much lower. The flow rate for all investigated system pressures is in the same range and shows at least for $p = 0.1$ MPa a similar course like the pressure difference. For higher pressure the flow rate is decreasing although the pressure difference shows a different trend. This can be explained by a reduction of the availability of water in the water pool with an increase of heat input and as a consequence a higher void fraction. It was proofed that for very high void fractions the water level is strongly fluctuating and the water level is even falling below the inlet of the natural circulation loop, which is located only 50 mm below the overflow.

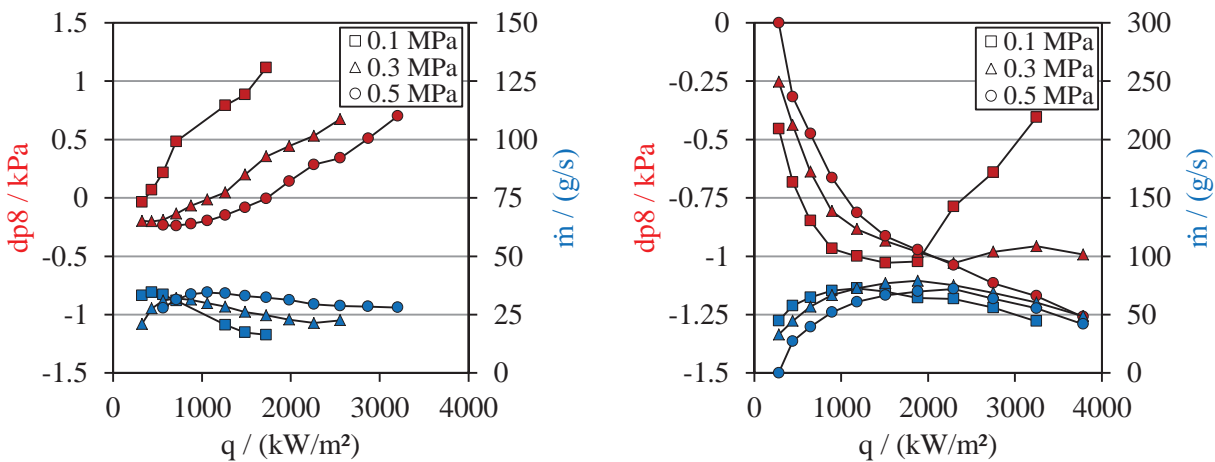


Figure 5. Axial pressure difference dp_8 and mass flow rate \dot{m} in the natural circulation loop vs. heat input q for cylinders (left) and screws (right)

4.3. Experimental Results at DHF Condition

Dryout experiments were carried out for all inflow conditions with variation of system pressure (0.1, 0.3 and 0.5 MPa). In order to determine the DHF the heat input is increased in small steps as it can be seen in Figure 6 for cylindrical particles under top-flooding condition. The first indication of an upcoming dryout in case of top-flooding is the reduction of pressure gradients in the bed. This effect starts at the bed's top (dp6) and propagates downwards (dp5, dp4). In the later course, a temperature excursion beyond saturation temperature can be observed. In some experiments, a temperature rise was detected by only one thermocouple, sometimes by six simultaneously. The DHF is assumed as the average of the heat input before reaching dryout and when dryout occurs.

The location of dryout is depicted in Figure 7. The markers symbolize the axial position of dryout for different inflow conditions and the markers' size represent the absolute frequency of dryout detection at a certain level. Here, no distinction is made between different system pressures since no dependency of system pressure on the position of dryout was observed. Furthermore, it was not taken into account that the number of thermocouples is different at each level. Thus, the probability of dryout detection is higher at a level with three thermocouples instead of one (see Figure 2).

For top-flooding, the dryout can be in the lower part of the bed since the dryout process starts at the top with a decrease of saturation, which can propagate downwards. In this stage the particles in the upper part are cooled by uprising steam with or without entrained droplets. In case of bottom-flooding (downcomer configuration 2, 3 and 5), the DHF mainly depends on the water inflow rate \dot{m} at the bottom, which in turn depends on the pressure gradients inside the debris bed. It is assumed that only very little water penetrates into the bed from top and only the upper particles can be cooled from top. Most of the particles are cooled by the injected water from the bottom. The dryout occurs, when the flow rate at the bottom falls below the evaporation rate. Therefore, dryout was detected in the upper part of the bed for these configurations. For the perforated downcomer configurations 4 and 6, the experiments have shown an inconsistent dryout position. In particular for screws with internal perforated downcomer, the position of dryout is quite low, whereas for the other configurations the dryout mainly occurs in the upper part. This can be attributed to multidimensional flow conditions, which can be established by a perforated downcomer.

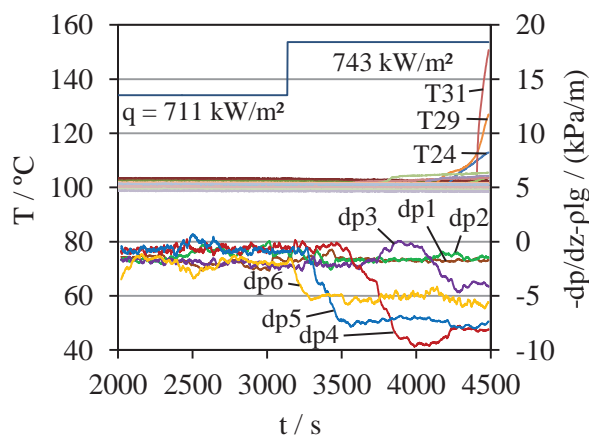


Figure 6. Dryout behavior for cylinders, top-flooding, $p = 0.1$ MPa

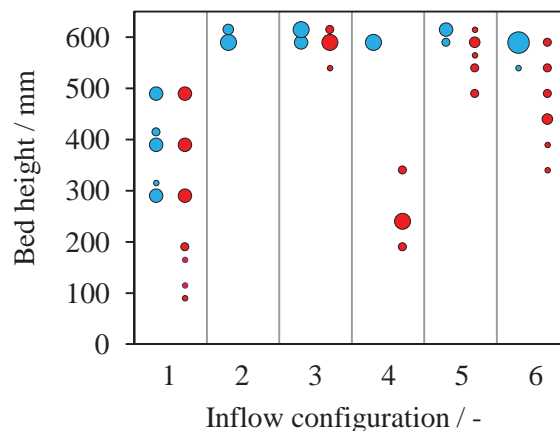


Figure 7. Position of dryout for cylinders (blue) and screws (red) for inflow configuration 1 - 6

Figure 8 and Table II show the determined DHFs for cylindrical particles and screws for all inflow configurations and applied system pressures. The error bars take into account the main uncertainties in the determination of the DHF, which are on the one hand the step size of heat input increase and on the other hand uncertainties regarding the determination of heat input and scattering in the experimental results. Additionally, due to the limited number of thermocouples in the bed an undetected hot spot in the bed can't be ruled out. For some bed configurations, it was not possible to reach dryout at 0.5 MPa, which is due to limitations of the inductive heating system. For the external downcomer, no DHF can be determined for screws. As mentioned before, the water level was strongly fluctuating for this configuration and thus the flow rate is not exclusively depending on the pressure gradient inside the bed but is limited by the available amount of water in the water pool. From the results it can be seen that the DHF is increasing with increasing pressure, which is mainly due to higher steam density at higher pressure. If the steam density is higher, a lower proportion of the flow cross-section is occupied by steam and the water penetration into the bed is improved.

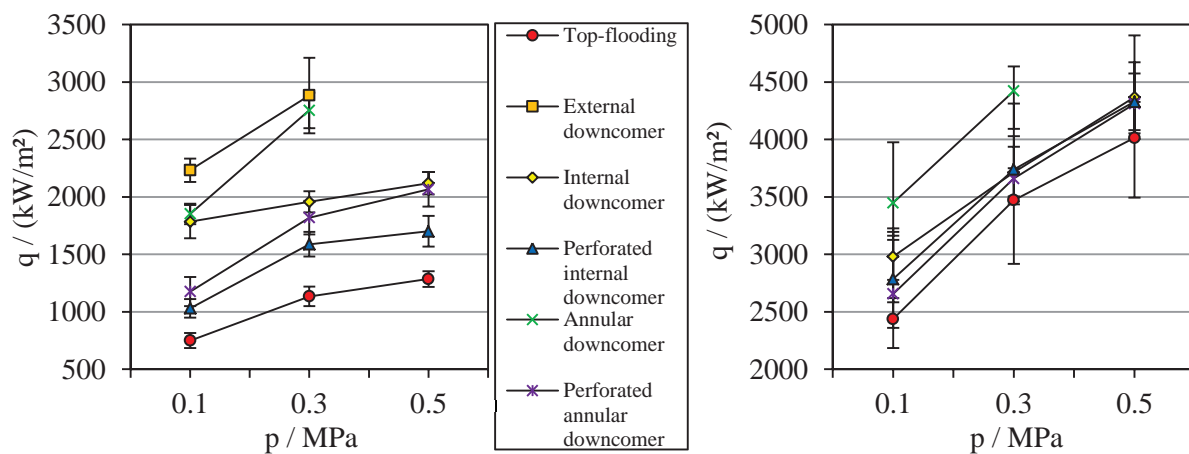


Figure 8. Dryout heat fluxes for cylinders (left) and screws (right) under variation of inflow condition

The comparison of both beds clearly illustrates the effect of the porosity on the coolability. At top-flooding, the DHF is a factor of 3.1 - 3.3 higher for screws ($\epsilon = 0.58$) than for cylinders ($\epsilon = 0.38$) at almost same effective particle diameters (bed 1: $d_p = 3.0$ mm; bed 2: $d_p = 2.8$ mm). The lowest DHF was determined for top-flooding since here water and steam are in counter-current flow and the coolability is limited by the CCFL. The results show that the DHF can be significantly increased by the installation of a downcomer, in particular for particles with low porosity. The highest increase was found for cylindrical particles with external downcomer, where the DHF is 2.5 - 3 times higher compared to top-flooding. Due to their low cross-sections the internal and annular downcomer configurations cannot increase the DHF to the same extent as the external downcomer. It turns out that the annular downcomer obtains a 3 - 41 % higher DHF than the internal downcomer. The reasons can be manifold. Firstly, the friction in the annular downcomer is lower since the cross-section is only reduced at the inlet (see section 3) and secondly water in the internal downcomer could be evaporated by heat transfer from the bed through the thin wall of the downcomer. Furthermore, pre-tests have shown that the DHF is not only limited by the minimal cross-section but also by the design of the downcomer's inlet. Possibly, a distribution of several small inlets has an advantage in terms of water inflow rate compared to one central inlet. The DHFs for the perforated downcomer configurations are quite close together. It can be assumed that previously mentioned reasons play no such significant role for these downcomers. For cylindrical particles, the DHF is only 32 - 61 % higher than for top-flooding and for screws even less (5 - 14 %). That a perforated downcomer obtains a

relatively poor coolability was also observed by Rashid et al. [3] in dryout tests and by Leininger et al. [14] for reflooding tests. Probably, the downcomer is blocked by uprising steam and therefore the DHF is lower than for the non-perforated versions.

Table II. Dryout heat fluxes and uncertainties / (kW/m²)

	Cylinders 3x5.75		
	0.1 MPa	0.3 MPa	0.5 MPa
Top-flooding	749 + 66 / - 66	1134 + 86 / - 86	1285 + 68 / - 68
External downcomer	2232 + 102 / - 102	2884 + 329 / - 329	no dryout reached
Internal downcomer	1784 + 145 / - 145	1957 + 92 / - 92	2120 + 98 / - 98
Perforated internal downcomer	1029 + 81 / - 81	1587 + 107 / - 107	1701 + 133 / - 133
Annular downcomer	1852 + 89 / - 89	2753 + 155 / - 155	no dryout reached
Perforated annular downcomer	1175 + 127 / - 127	1818 + 146 / - 146	2065 + 151 / - 151

	Screws M3x10		
	0.1 MPa	0.3 MPa	0.5 MPa
Top-flooding	2437 + 183 / - 253	3472 + 278 / - 555	4014 + 311 / - 521
External downcomer	no dryout can be determined		
Internal downcomer	2980 + 216 / - 203	3713 + 223 / - 207	4368 + 305 / - 287
Perforated internal downcomer	2784 + 443 / - 202	3740 + 573 / - 281	4328 + 577 / - 275
Annular downcomer	3448 + 528 / - 287	4422 + 213 / - 329	no dryout reached
Perforated annular downcomer	2656 + 470 / - 296	3660 + 369 / - 226	4311 + 263 / - 308

5. CONCLUSIONS

Boiling and dryout experiments were carried out in the DEBRIS test facility for two homogeneous beds with different porosity (cylinders – $\varepsilon = 0.38$, screws – $\varepsilon = 0.58$) under variation of inflow condition. The boiling experiments pointed out the influence of inflow condition on the pressure gradients inside the debris bed. In case of bottom-flooding, the flow rate in the external loop was measured and the relation to pressure gradients inside the bed was illustrated. Here, the effect of different porosity was clearly visible. For cylindrical particles, the pressure gradients were higher and thus the mass flow rates and coolability lower than for screws.

The dryout experiments have shown that in case of top-flooding a dryout can be indicated by a pressure drop inside the bed followed by a temperature excursion. For bottom-flooding by a downcomer, it is remarkable that the dryout occurs in the upper part of the bed since the bed is mainly cooled by the injected water at the bottom and only partly by the water penetration from top. An uneven picture emerges for perforated downcomers, where dryout mainly occurs in the upper part but also in the middle part of the bed.

The comparison of two beds with strong difference in porosity has confirmed the forceful influence of the porosity on the coolability. By the installation of a downcomer the DHF can be increased by a factor of up to 3.3 compared to pure top-flooding. The highest DHF was determined for the external downcomer,

which has the highest flow cross-section followed by the annular and the internal downcomer. The perforated internal and annular downcomers show only a slight increase in DHF.

ACKNOWLEDGMENTS

This work was funded by the German Federal Ministry of Economic Affairs and Energy under grant number 1501466 on the basis of a decision by the German Bundestag.

REFERENCES

1. G. Hofmann, "On the location and mechanisms of dryout in top-fed and bottom-fed particulate beds", *Nuclear Technology*, **Vol. 65**, pp. 36-45 (1984).
2. P. Schäfer, M. Groll, R. Kulenovic, "Basic investigations on debris cooling", *Nuclear Engineering and Design*, **236** (19-21), pp. 2104-2116 (2006).
3. M. Rashid, R. Kulenovic, E. Laurien, "Experimental results on the coolability of a debris bed with down comer configurations", *Nuclear Engineering and Design*, **249**, pp. 104-110 (2012).
4. A. Kaiser, W. Schütz, H. Will, "PREMIX experiments PM12-PM18 to investigate the mixing of a hot melt with water", FZKA-6380, Forschungszentrum Karlsruhe GmbH, Karlsruhe, Germany, (2001).
5. K. Atkhen, G. Berthoud, "SILFIDE experiment: Coolability in a volumetrically heated debris bed", *Nuclear Engineering and Design*, **236** (19-21), pp. 2126-2134 (2006).
6. L.X. Li, W.M. Ma, S. Thakre, "An experimental study on pressure drop and dryout heat flux of two-phase flow in packed beds of multi-sized and irregular particles", *Nuclear Engineering and Design*, **242**, pp. 369-378 (2012).
7. M.J. Konovalikhin, I.V. Kazachkov, B.R. Sehgal, "Dryout heat flux in a low porosity volumetrically heated particle bed", *4th International Conference on Multiphase Flows*, New Orleans, LA, USA, May (2001).
8. A. Nayak, B. Sehgal, A. Stepanyan, "An experimental study on quenching of a radially stratified heated porous bed", *Nuclear Engineering and Design*, **236** (19-21), pp. 2189-2198 (2006).
9. Z.L. Yang, B.R. Sehgal, "Cooling of an internal-heated debris bed with fine particles", *9. International Conference on Nuclear Engineering*, Nice, France 8-12 April (2001).
10. N. Chikhi, O. Coindreau, L.X. Li, W.M. Ma, V. Taivassalo, E. Takasuo, S. Leininger, R. Kulenovic, E. Laurien, "Evaluation of an effective diameter to study quenching and dry-out of complex debris bed", *Annals of Nuclear Energy*, **74**, pp. 24-41 (2014).
11. B.W. Spencer, K. Wang, C.A. Blomquist, L.M. McUmbler, J. P. Schneider, "Fragmentation and quench behavior of corium melt streams in water", (No. NUREG/CR--6133; ANL--93/32), Argonne National Laboratory, Argonne, Illinois, United States (1994).
12. A. Karbojian, W.M. Ma, P. Kudinov, T.N. Dinh, "A scoping study of debris bed formation in the DEFOR test facility", *Nuclear Engineering and Design*, **239** (9), pp. 1653-1659 (2009).
13. S. Ergun, "Fluid flow through packed columns", *Chemical Engineering Progress*, **48** (2), pp. 89-94 (1952).
14. S. Leininger, R. Kulenovic, S. Rahman, G. Repetto, E. Laurien, "Experimental investigation on reflooding of debris beds", *Annals of Nuclear Energy*, **74**, pp. 42-49 (2014).